Journal of Catalysis **188,** 393–402 (1999)
Article ID jcat.1999.2670, available online at http://www.idealibrary.com on IDEAL®

Methane Dehydro-aromatization over Mo/HZSM-5 in the Absence of Oxygen: A Multinuclear Solid-State NMR Study of the Interaction between Supported Mo Species and HZSM-5 Zeolite with Different Crystal Sizes

Weiping Zhang, Ding Ma, Xiuwen Han, Xiumei Liu, Xinhe Bao,[1] Xinwen Guo,* and Xiangsheng Wang*

*State Key Laboratory of Catalysis, Dalian Institute of Chemical Physics, Chinese Academy of Sciences, 457 Zhongshan Road, P.O. Box 110, Dalian 116023, China; and * Laboratory of Comprehensive Utilization of Carbonaceous Resources, Dalian University of Technology, Dalian 116012, China*

Received June 16, 1999; revised August 30, 1999; accepted August 30, 1999

The interaction between Mo species and a conventionally microsized and particularly nanosized HZSM-5 support was studied by high-resolution multinuclear solid-state NMR techniques. As proved by ^{27}Al and ^{29}Si MAS as well as CP/MAS NMR investigations, this interaction was so strong that the framework aluminum of both microsized and nanosized HZSM-5 zeolites could be extracted. With increasing Mo loading, more nonframework aluminum, resonanced at ca. 30 ppm, appeared in the ^{27}Al MAS NMR spectrum of the Mo-loaded nanosized HZSM-5 catalyst. Meanwhile, this strong interaction led to the formation of more new $Al_2(MoO_4)_3$ crystallines on the nanosized HZSM-5 support than on the microsized HZSM-5 support. The appearance of $Al_2(MoO_4)_3$ crystallines resulted in fewer active catalysts for the methane dehyro-aromatization. The results of ^{1}H MAS NMR using perfluorotributyl amine as a probe molecule demonstrated that Mo species preferentially reacted with the silanols and nonframework AlOH on the external surface of microsized and nanosized HZSM-5 zeolites. In addition, impregnated Mo species remained predominantly on the external surface of the nanosized HZSM-5 zeolite, although there was a possibility that they might migrate into the lattice channels of the microsized HZSM-5 zeolite. The migration of some Mo species into the zeolite channels might be beneficial for the conversion of methane to aromatics in the absence of oxygen.

Key Words: **solid-state NMR; Mo/HZSM-5; nanosized HZSM-5 zeolite; methane activation; probe molecule; perfluorotributyl amine.**

1. INTRODUCTION

The activation of methane to form desired commercial chemicals is a great challenge to catalysis science. In recent years, the catalytic conversion of methane to higher hydrocarbons, especially to aromatics such as benzene, toluene, and naphthalene, in the absence of oxygen was extensively studied (1–13). In 1993, Wang and Xu *et al.* of our laboratory first reported the dehydrogenation and aromatization of methane in the absence of oxygen on a transition metal ion-modified HZSM-5 zeolite catalyst (1). Among the tested catalysts, Mo/HZSM-5 is the best. Similar catalytic performances have been obtained by other research groups for methane aromatization. After impregnation of the HZSM-5 zeolite with ammonium heptamolybdate (AHM) solution and calcination, Xu *et al.* (2, 3) observed clear decrease in the BET surface area and strong acidity of HZSM-5; they suspected that interactions occur between the Mo species and the HZSM-5 support. XRD, FT-IR, and MAS NMR investigations also showed that the formation of MoO_3 and $Al_2(MoO_4)_3$ crystallines depends on the Mo loading and the calcination temperature (2, 3, 8, 10). It can be deduced that certain interactions exist between the supported Mo species and the HZSM-5 zeolite during catalyst preparation. However, this kind of interaction has not been discussed in the literature.

It is well known that multinuclear solid-state magic-angle spinning nuclear magnetic resonance (MAS NMR) is a powerful technique for studying the structure of molecular sieves and other heterogeneous catalysts (14, 15). ^{27}Al and ^{29}Si MAS NMR can provide unique and detailed information on zeolite structures and properties and can discriminate between framework Al and nonframework Al and determine the coordinating modes of aluminum atoms to silicon atoms, etc. The cross-polarization (CP) technique may be used for signal enhancement and the detection of protons closely connected to the aluminum or silicon atom, i.e., nonframework AlOH and SiOH groupings. ^{1}H MAS NMR spectroscopy is a direct and senstitive tool for characterizing the local environment of protons in zeolites; different acidic sites can be distinguished by chemical shifts induced by selective adsorption of certain probe molecules

[1] To whom correspondence should be addressed. Fax: 0086-411-4694447. E-mail: xhbao@ms.dicp.ac.cn.

0021-9517/99 $30.00

(16, 17). In our study, two sizes of crystals—conventionally microsized and particularly nanosized HZSM-5 zeolites—were used as the support in order to shed light on the nature of the interaction between the Mo species and the HZSM-5 support. A multinuclear solid-state NMR study, including ^{27}Al and ^{29}Si MAS and CP/MAS NMR and ^{1}H MAS NMR, was performed to evaluate this type of interaction. By selective adsorption of perfluorotributyl amine, the distribution of Brønsted acidity and Mo species between the internal and external surface of the zeolite can be identified. This kind of distribution, which originates from the interaction between the Mo species and the HZSM-5 zeolite, is probably related to the high activity of the Mo/HZSM-5 catalyst in the conversion of methane to aromatics under nonoxidative conditions.

2. EXPERIMENTAL

2.1. Catalyst Preparation

NaZSM-5 zeolite with controlled crystal sizes was prepared by varying the duration and temperature of crystallization as well as the amount of alkali metal salt such as NaCl (18). Fully exchanged HZSM-5 with a Si/Al ratio of 28 was obtained by ion exchange of NaZSM-5 with a 0.4 M aqueous solution of ammonium nitrate at 353 K for 2 h, followed by drying at 393 K and calcining at 773 K. As described in our previous paper (18), the crystal sizes of the resultant samples were 1000 and 70 nm, respectively, as determined by the transmission electron microscope (TEM); they were denoted as *micro*-HZ and *nano*-HZ, respectively. Catalysts with Mo loadings of 2, 6, and 15 wt% were obtained by impregnating the above HZSM-5 zeolites with an aqueous solution of ammonium heptamolybdate (AHM) of appropriate concentration. The samples were then dried at 373 K for 8 h and calcined in air for 5 h at 773 K. Prior to the $^{1}H \rightarrow {}^{27}$Al CP/MAS NMR measurements, the samples were hydrated completely in a desiccator with saturated NH_4NO_3 (19, 20).

2.2. NMR and XRD Measurements

A special device, which is functionally analogous to the CAVERN apparatus developed by Haw and coworkers (17, 21), was employed for the on-line zeolite sample treatments. After dehydration and exposure to adsorbates, the samples can be filled *in situ* into an NMR rotor, sealed, and transferred to the spectrometer without exposure to air. In the present experiment, the zeolites were dehydrated typically at 673 K and at a pressure below 10^{-2} Pa for 10–20 h before the ^{1}H MAS NMR measurements. Selective adsorption of perfluorotributyl amine (from Acros Organics) was performed by exposing the dehydrated sample to its saturated vapor at room temperature for 30 min, and then degassing it at 298 K to remove the physical adsorbates from the surface.

All NMR spectra were collected at room temperature on a Bruker DRX-400 spectrometer with a BBO MAS probe using 4-mm ZrO_2 rotors. ^{29}Si MAS NMR spectra were recorded at 79.5 MHz using a 0.8-μs $\pi/8$ pulse with a 4-s recycle delay and 2000 scans. $^{1}H \rightarrow {}^{29}$Si CP/MAS NMR experiments were performed with a 4-s recycle delay, 4000 scans, and a contact time of 1.5 ms. All ^{29}Si spectra were recorded on samples spun at 4 kHz, and chemical shifts were referenced to 4,4-dimethyl-4-silapentane sulfonate sodium (DSS). ^{27}Al MAS NMR spectra were recorded at 104.3 MHz using a 0.75-μs $\pi/12$ pulse with a 3-s recycle delay and 400 scans. $^{1}H \rightarrow {}^{27}$Al CP/MAS spectra were recorded with a single contact, an optimized contact time of 1.2 ms, a recycle delay of 3 s, and 8000 to 10,000 scans. The Hartmann–Hahn condition was established in one scan on a sample of high quality kaolinite under similar conditions. Only the central $(+1/2 \leftrightarrow -1/2)$ transition was observed; thus excitation in the $^{1}H \rightarrow {}^{27}$Al CP/MAS experiment is selective, and the Hartmann–Hahn condition is $3\gamma_{Al}B_{Al} = \gamma_{H}B_{H}$ (22, 23). ^{1}H MAS NMR spectra were collected at 400.1 MHz using single-pulse experiments with 1 μs $\pi/10$ pulse, a 4-s recycle delay, and 200 scans. Both ^{27}Al and ^{1}H MAS NMR spectra were recorded with samples spun at 8 kHz, and chemical shifts were referenced to 1% aqueous $Al(H_2O)_6^{3+}$ and to a saturated aqueous solution of DSS, respectively. The Bruker software WINNMR was employed for deconvolution using fitted Gaussian-Lorentzian line shapes.

X-ray diffraction patterns were obtained at room temperature on a Rigaku D/max-γb X-ray diffractometer using monochromatic Cu$K\alpha$ radiation (40 kV and 100 mA). Power diffractograms of the samples were recorded over a range of 2θ values from 5 to 50° at a scanning rate of 5°/min.

2.3. Catalytic Test

Methane aromatization reactions were performed under nonoxidative conditions in a fixed bed continuous-flow quartz reactor at 973 K and at atmospheric pressure. In brief, 0.2 g catalyst (20–60 mesh) was heated to 973 K for 1 h in a stream of He (UHP) and was maintained at 973 K for 30 min, before introducing methane. The reaction mixture was analyzed by an on-line gas chromatography (Shimadzu GC-9A) using TCD as the detector. Ten percent N_2/CH_4 (UHP) was used as an internal standard so that the conversion of methane could be determined accurately and the coke formation during the reaction could be evaluated on the basis of carbon number balance (6, 9, 11, 12).

3. RESULTS AND DISCUSSION

3.1. ^{27}Al MAS and $^{1}H \rightarrow {}^{27}$Al CP/MAS NMR

^{27}Al MAS NMR spectra can yield more valuable information on the structure of zeolites. Chemical shifts enable

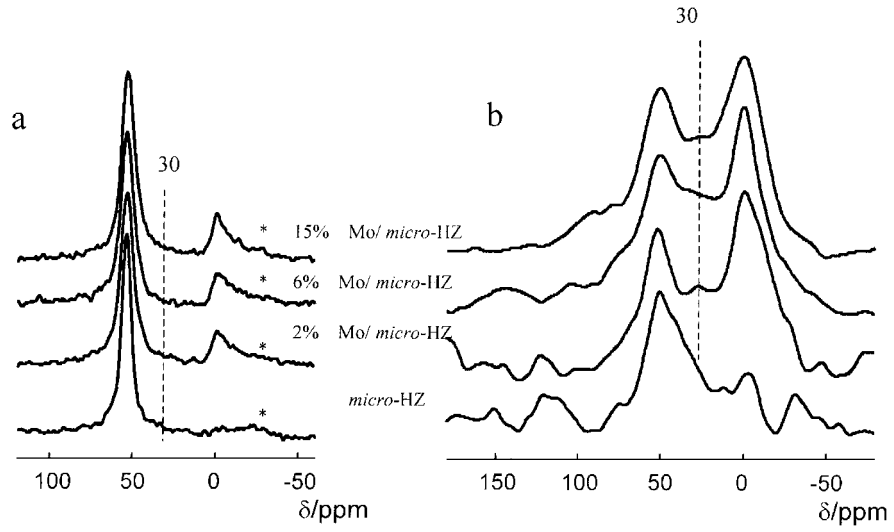

FIG. 1. ^{27}Al MAS (a) and $^{1}H \rightarrow {}^{27}$Al CP/MAS (b) NMR spectra of the microsized HZSM-5 zeolite with different Mo loadings. Prior to CP/MAS NMR measurements, samples were completely hydrated in a desiccator with saturated NH_4NO_3. The resonance at *ca.* 30 ppm is an independent signal and may be ascribed to pentacoordinated nonframework aluminum. Asterisks denote MAS side bands.

discrimination between framework (tetrahedrally coordinated) and nonframework (octahedrally or pentacoordinated) aluminum (19, 20, 24). Combined with $^{1}H \rightarrow {}^{27}$Al CP/MAS NMR, it can give further insights into the nature of the nonframework Al species. Figures 1a and 2a show the ^{27}Al MAS NMR spectra of microsized and nanosized HZSM-5 zeolites loaded with Mo that were hydrated saturatedly in air. There are two main peaks, as expected; one at 52 ppm is typically associated with four-coordinated framework aluminum in ZSM-5 zeolite, and the other at 0 ppm is commonly attributed to octahedral nonframework aluminum. With increasing Mo loading, the peak intensity

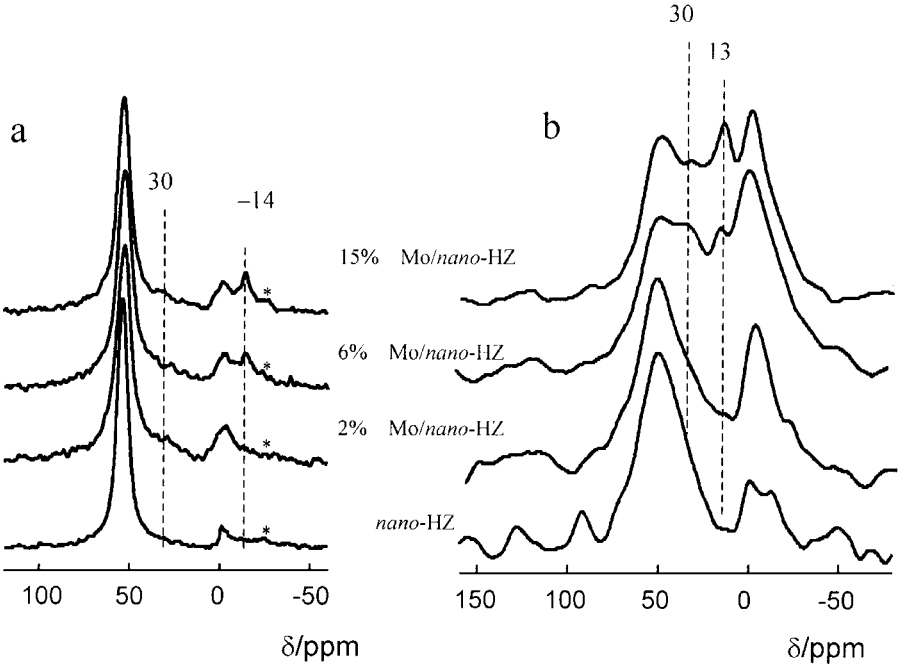

FIG. 2. ^{27}Al MAS (a) and $^{1}H \rightarrow {}^{27}$Al CP/MAS (b) NMR spectra of the nanosized HZSM-5 zeolite with different Mo loadings. After introducing the Mo species, a new signal at *ca.* −14 ppm appears in the ^{27}Al MAS NMR spectra which is attributed to the octahedral aluminum in crystalline $Al_2(MoO_4)_3$. However, it may be hydrolyzed after the samples were completely hydrated and gives a signal resonanced at *ca.* 13 ppm in the $^{1}H \rightarrow {}^{27}$Al CP/MAS NMR spectra. Asterisks denote MAS side bands.

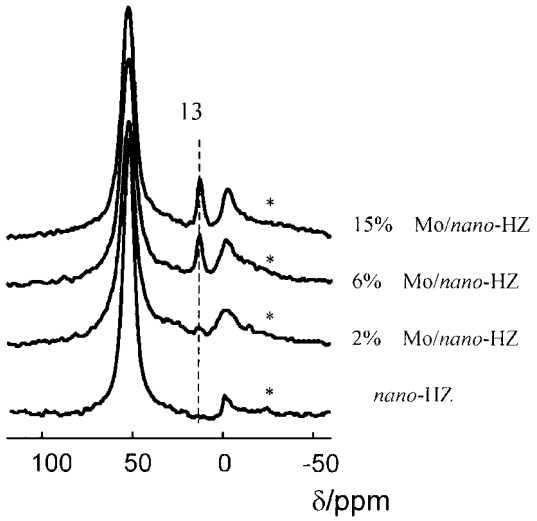

FIG. 3. ^{27}Al MAS NMR spectra of the Mo-loaded nanosized HZSM-5 zeolite recorded after the samples completely hydrated in a desiccator with saturated NH_4NO_3. Asterisks denote MAS side bands.

of the framework Al decreases, while its line width at half height broadens. At the same time, the amount of nonframework Al at 0 ppm increases. Compared to the microsized HZSM-5 as the support, the introduction of Mo species on the nanosized HZSM-5 support increases the intensity of the peak at about 30 ppm, which may be assigned to pentacoordinated nonframework Al (20, 24) (Fig. 2a). These facts reveal that the Mo species interact with framework Al and dealuminate the framework. However, for both the microsized and nanosized HZSM-5, the thermal stability of the framework hardly changes when the Mo-loading increases from 2 to 15 wt%. However, a new peak at about −14 ppm appears sharply as Mo-loading increases (Figure 2a). This peak is attributed to octahedral aluminum in crystalline $Al_2(MoO_4)_3$ (8, 10), which is related to the introduction of the Mo species. It can be seen from comparing Figs. 1a and 2a that the formation of $Al_2(MoO_4)_3$ will occur more readily when the crystal size of HZSM-5 zeolite is reduced to the nanoscale. This new $Al_2(MoO_4)_3$ crystalline phase was also detected by XRD on the Mo-loaded nanosized HZSM-5 zeolite (Fig. 4). In addition, the ^{27}Al quadrupolar nuclei ($I = 5/2$) is very sensitive to its local environment. Therefore, the increase in the line width of framework Al in the ^{27}Al MAS NMR spectra implies that the introduction of the Mo species causes a strong electrical field gradient at the nucleus; thus, the location of the Mo species is associated with framework Al. This will be discussed further in Section 3.3.

The application of the $^1H \rightarrow {}^{27}Al$ cross-polarization technique can selectively enhance the Al signals of aluminum atoms which are coupled with protons of hydroxyl groups by ^1H–^{27}Al dipolar interaction. Figures 1b and 2b show the $^1H \rightarrow {}^{27}Al$ CP/MAS NMR spectra of samples hydrated completely in a desiccator with saturated NH_4NO_3. It is clearly demonstrated that the signals at about 0 and 30 ppm increase after cross-polarization, while the signal at 52 ppm decreases. This indicates that the aluminum at these two positions (52 and 30 ppm) is located in different chemical environments and interacts with different protons of hydroxyl groups. Thus, the resonance at *ca.* 30 ppm is an independent signal associated with nonframework Al, which is not part of the second-order quadruple line shape as reported by Samoson (25). The compositions of nonframework Al are $[Al(OH)_n]^{3-n}$, $Al(H_2O)_6^{3+}$, and aluminas (26, 27). As indicated in the $^1H \rightarrow {}^{27}Al$ CP/MAS and MAS NMR spectra, after loading the Mo species, the amount of nonframework Al at *ca.* 30 ppm seems to increase when the crystal

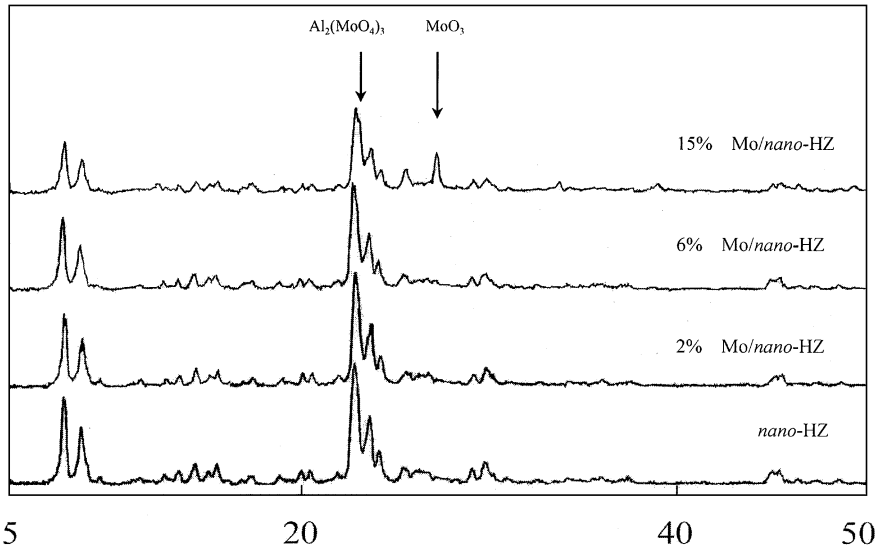

FIG. 4. XRD patterns of the nanosized HZSM-5 zeolite with different Mo loadings.

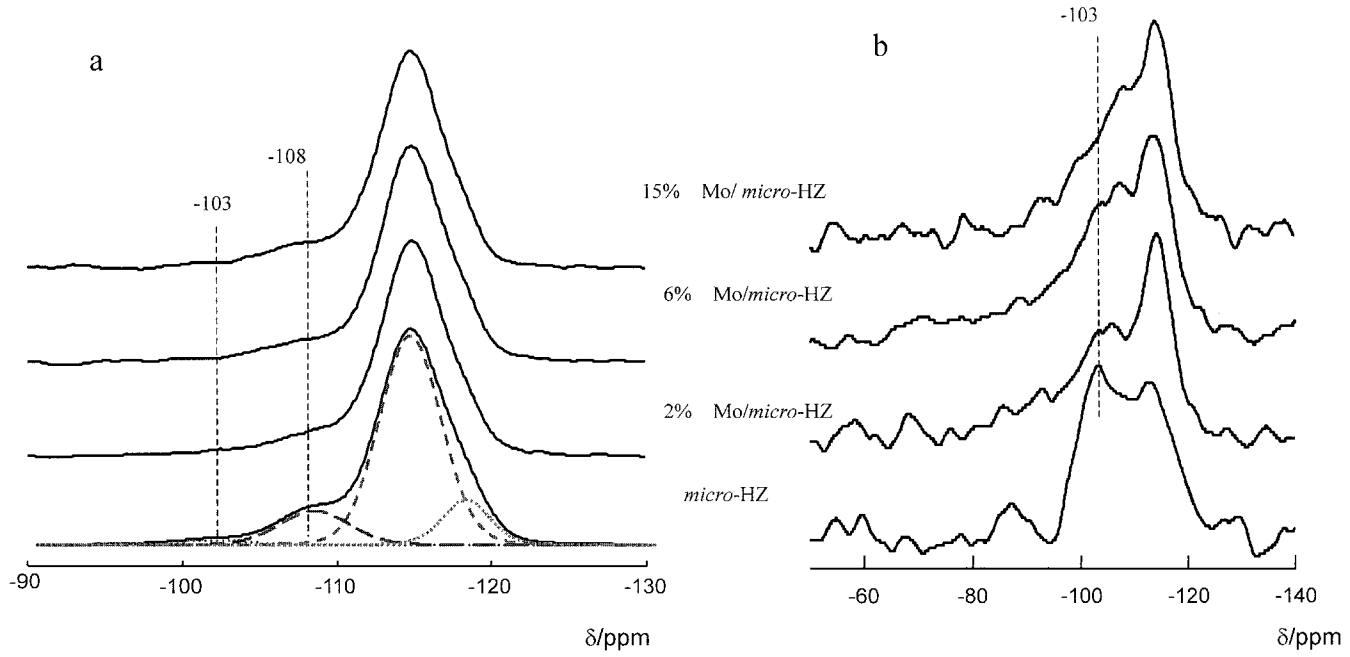

FIG. 5. ^{29}Si MAS (a) and $^{1}H \rightarrow {}^{29}$Si CP/MAS (b) NMR spectra of the microsized HZSM-5 zeolite with different Mo loadings. The ^{29}Si MAS NMR spectra can be deconvoluted using four Gaussian–Lorentzian lines. The signal at −103 ppm in the $^{1}H \rightarrow {}^{29}$Si CP/MAS NMR spectra can be enhanced selectively because the silicon atoms are connected to the hydroxyl groups.

size of the HZSM-5 support is reduced to the nanoscale. Moreover, a new peak at *ca.* 13 ppm was observed only in the $^{1}H \rightarrow {}^{27}$Al CP/MAS NMR spectra of the Mo-loaded nanosized HZSM-5 catalysts (Fig. 2b). The corresponding ^{27}Al MAS NMR spectra of the nanosized samples, hydrated completely in a desiccator, are shown in Fig. 3. Obviously, when compared with Fig. 2a (samples were hydrated saturatedly in air), the resonance signal of $Al_2(MoO_4)_3$ at −14 ppm disappeared, while a new sharp peak at *ca.* 13 ppm appeared. This confirms that $Al_2(MoO_4)_3$ crystallines formed on the nanosized HZSM-5 zeolite may be hydrolyzed under the completely hydrated conditions. This signal at *ca.* 13 ppm will be enhanced after cross-polarization (Fig. 2b). Thus, we tend to attribute the signal at *ca.* 13 ppm (Fig. 3) to octahedral nonframework Al in $MoO_3 \cdot Al_2O_3 \cdot nH_2O$ (n is the coordination number of H_2O, $n > 1$) (28). However, this signal was not observed in the $^{1}H \rightarrow {}^{27}$Al CP/MAS NMR spectra of Mo-loaded microsized HZSM-5 catalysts (Fig. 1b) and their corresponding MAS NMR spectra of samples hydrated completely (the spectra are not shown here). Hence, these new $Al_2(MoO_4)_3$ crystallines are more stable on the microsized than on the nanosized HZSM-5 zeolites.

The above results show that the Mo species interact with framework aluminum of the HZSM-5 zeolite and lead to dealumination of the framework. For the nanosized HZSM-5 support, this interaction will be more severe and result in more nonframework aluminum, appearing at *ca.* 30 ppm in the ^{27}Al MAS NMR spectrum. This strong interaction seems to increase with increasing Mo loading and finally leads to the formation of new $Al_2(MoO_4)_3$ crystallines. The stability of these new crystallines, formed on the nanosized HZSM-5 zeolite, is different from that on the microsized zeolite.

3.2. ^{29}Si MAS and $^{1}H \rightarrow {}^{29}$Si CP/MAS NMR

The ^{29}Si MAS NMR spectra of the samples and their corresponding $^{1}H \rightarrow {}^{29}$Si CP/MAS NMR spectra are indicated in Figs. 5 and 6. After the curve is deconvoluted by Gassian and Lorentzian line shapes, four peaks are clearly seen in the ^{29}Si MAS NMR spectrum. The peaks at −114 and −108 ppm stem from the Si (0 Al) and Si (1 Al) groupings. The shoulder peak at about −117 ppm is commonly attributed to the crystallographically inequivalent sites of Si (0 Al) groupings (29). Figures 5a and 6a seem to show that the peak intensity at −108 ppm decreases with increasing Mo loading. According to Loewenstein's rule (30), the framework Si/Al ratio can be calculated from the peak areas in the ^{29}Si MAS NMR spectrum (31), and the results are listed in Table 1. The Si/Al ratio increases gradually with Mo loading. These facts reveal that the introduction of the Mo species causes the dealumination of the HZSM-5 framework; this interaction becomes stronger with increasing Mo loading.

The peak at −103 ppm in the ^{29}Si MAS NMR spectrum can be assigned to the silanols in $[Si(OH)(OSi)_3]$ groupings. As demonstrated in Figs. 5b and 6b, this peak is selectively enhanced when the $^{1}H \rightarrow {}^{29}$Si cross-polarization

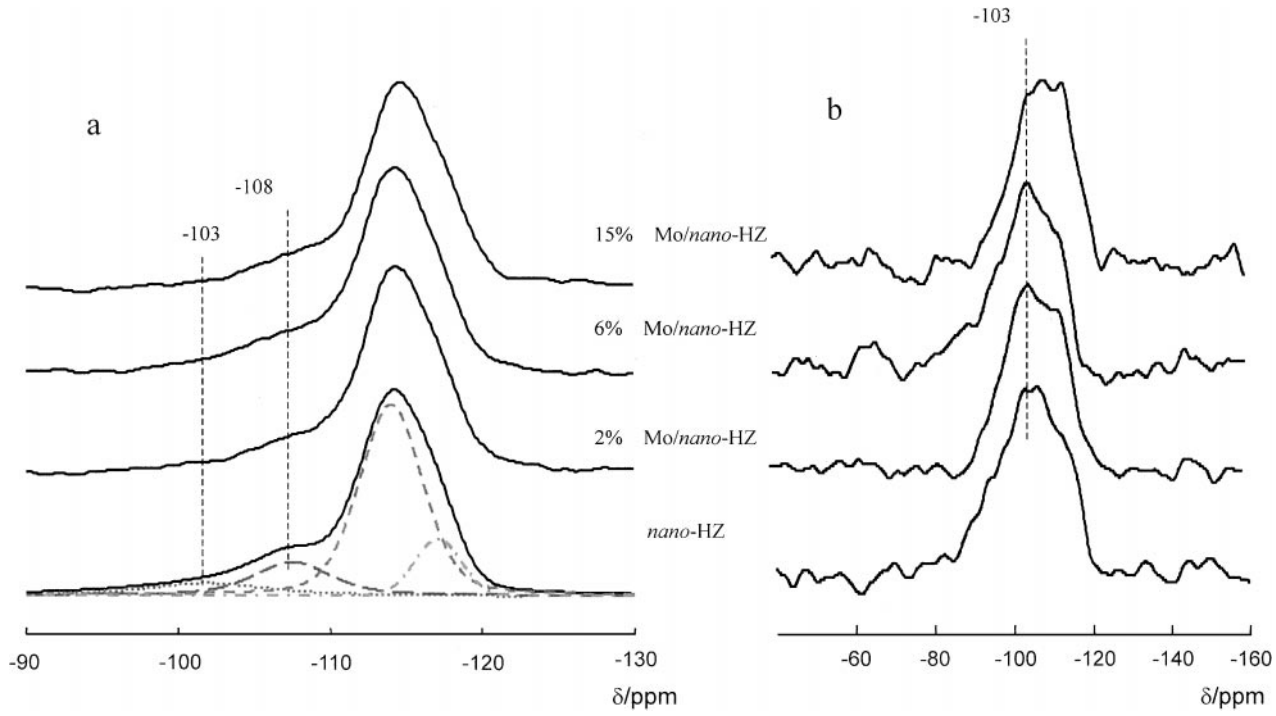

FIG. 6. ^{29}Si MAS (a) and ^{1}H → ^{29}Si CP/MAS (b) NMR spectra of the nanosized HZSM-5 zeolite with different Mo loadings.

technique is used. The concentration of the silanol groups with respect to the total number of Si atoms can be obtained by integrating the above deconvoluted MAS NMR spectra (Table 1). For the nanosized HZSM-5 zeolite, the concentration of the silanols is distinctly higher (11%) than that of the microsized HZSM-5 zeolite (3.2%). After being loaded with Mo, the concentration of the silanols obviously decreases, especially that of the microsized HZSM-5 zeolite (see ^{1}H → ^{29}Si CP/MAS NMR spectra in Fig. 5b). For example, when Mo loading reaches 15 wt%, only 0.5% silanols are left on the microsized HZSM-5 support, while for the nanosized HZSM-5 support, the concentration of the silanols is 1.5%. These results indicate that the Mo species react with the silanols on the HZSM-5 support to reduce its concentration. The same result was achieved in the following ^{1}H MAS NMR experiments.

3.3. *^{1}H MAS NMR*

High-resolution ^{1}H MAS NMR, a useful and direct method, has been employed routinely to characterize the acidic sites in zeolites. Compared with IR, it can provide quantitative information on the interaction between the supported metal ions and the hydroxyl species on the

TABLE 1

Si/Al Ratio, Concentration of Silanols, External Brønsted Acidic Sites, and Nonframework AlOH of the Mo/*micro*-HZ and Mo/*nano*-HZ Catalysts Measured by ^{29}Si MAS and ^{1}H MAS NMR Spectra

Catalysts	Micro-sized HZSM-5	2 wt% Mo/ *micro*-HZ	6 wt% Mo/ *micro*-HZ	15 wt% Mo/ *micro*-HZ	Nano-sized HZSM-5	2 wt% Mo/ *nano*-HZ	6 wt% Mo/ *nano*-HZ	15 wt% Mo/ *nano*-HZ
Si/Al ratio	28.9	33.1	34.1	33.9	28.3	31.1	31.5	34.6
Concentration of silanols (%)	3.2	1.4	0.6	0.5	11.0	4.7	2.7	1.5
Concentration of external Brønsted acidic sites (%)	3.5	2.9	2.8	2.5	31.7	23.3	8.5	4.7
Concentration of external nonframework AlOH (%)	53.1	44.1	42.9	35.2	65.6	55.7	51.1	28.2

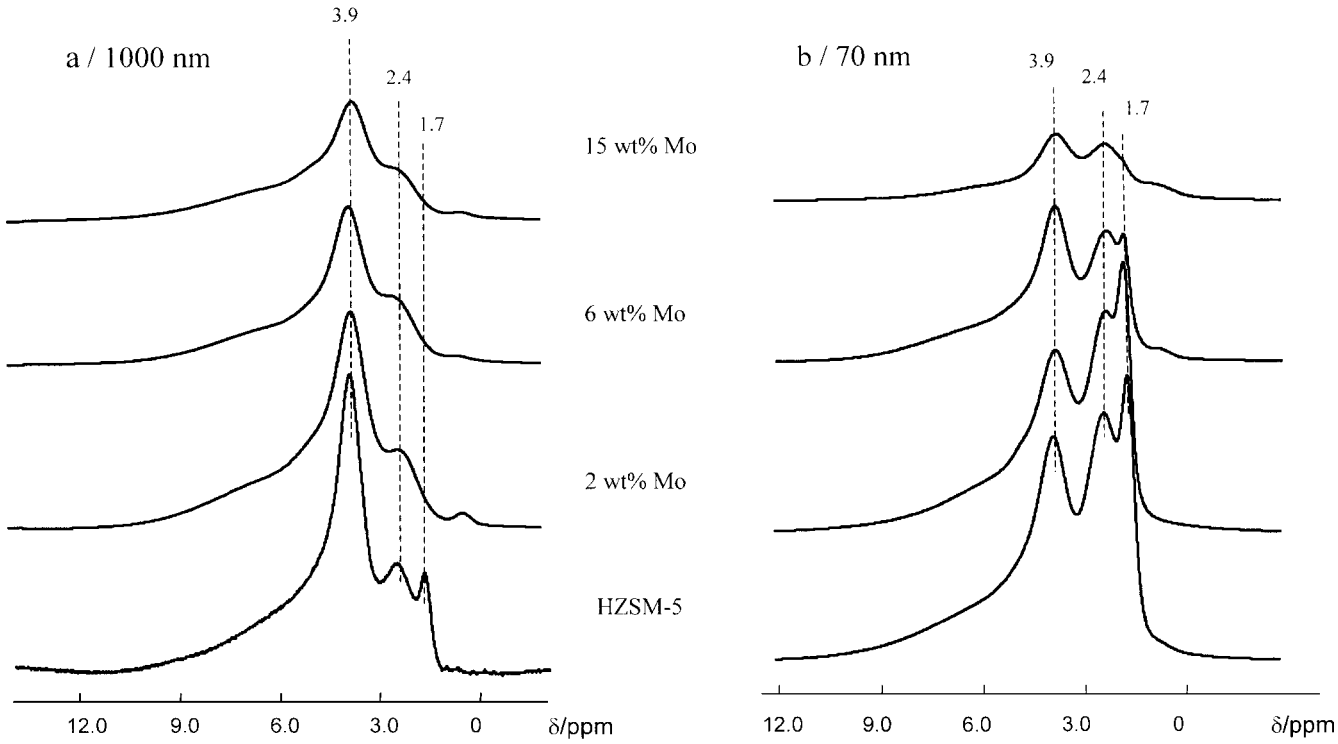

FIG. 7. ^{1}H MAS NMR spectra of the microsized (a) and the nanosized (b) HZSM-5 zeolites with different Mo loadings, recorded at a resonance frequency of 400.1 M Hz with a sample spinning rate of 8 kHz and 200 scans.

catalyst surface without the difficulties associated with extinction coefficients. Figure 7 displays the ^{1}H MAS NMR spectra of the HZSM-5 zeolite with different Mo loadings. As demonstrated, the peaks centered at about 1.7 and 3.9 ppm are assigned to the nonacidic hydroxyl groups (silanols) and bridging hydroxyl groups (Brønsted acidic sites), respectively, while the resonance at about 2.4 ppm is attributed to hydroxyl groups bonded to the extraframework aluminum (16, 32). However, a broad peak at about 5.8 ppm can be identified in the deconvoluted ^{1}H MAS NMR spectra (Fig. 8). It is ascribed to a second Brønsted acidic site in HZSM-5 zeolites, which interacts electrostatically with the zeolite framework (16, 32, 33). In addition, the signal at about 4.9 ppm may be associated with an extremely small number of water molecules that reside in the zeolite cages (34). Figure 7 seems to show, for both the microsized and the nanosized HZSM-5 zeolites, that the total ^{1}H signal intensity decreases upon loading Mo and the signals at 1.7 and 2.4 ppm are preferentially reduced compared to that at 3.9 ppm. These signals reveal that, during sample preparation, the impregnated Mo species react with the nonacidic silanols and nonframework AlOH groups on the surface of the zeolites. A similar reaction between Al–OH species and $Mo_7O_{24}^{6-}$ anionic species was proposed during the preparation of Mo/Al_2O_3 catalysts (35, 36).

Perfluorotributyl amine [$(n\text{-}C_4F_9)_3N$] is a weak base with a diameter of 0.94 nm (37), which is much larger than the pore size of microporous zeolites such as ZSM-5 (0.55 nm) and Y (0.74 nm) zeolites. We found that it is a sensitive NMR probe for quantitative determination of external acidity as well as for determining the position of silanols and some nonframework Al species in zeolites by ^{1}H MAS NMR spectroscopy (38). Figure 8 shows the ^{1}H MAS NMR spectra of nanosized HZSM-5 zeolite before (top curve) and after (bottom curve) adsorption of perfluorotributyl amine. Quantitative deconvolution of the corresponding spectra are plotted simultaneously. After adsorption of perfluorotributyl amine the resonance position of silanols shifts 0.2 ppm to the low-field, revealing that most of the silanols are located on the external surface and not at the lattice defects in the internal surface. The peak intensity at 3.9 ppm decreases, while that at about 5.8 ppm increases. This suggests that a portion of the Brønsted acidic sites, which are located on the external surface of the zeolites react with the perfluorotributyl amine to form a perfluorotributyl aminium ion, the resonance signal of which appears at about 6.0 ppm. However, the Brønsted acidic sites on the internal surface are not accessible to perfluorotributyl amine, and their chemical shift is unchanged. Similar variation is observed for nonframework AlOH. After adsorption of perfluorotributyl amine, the 0.3 ppm low-field shift of the signal at 2.4 ppm demonstrates that some of the nonframework Al exists on the external surface of the zeolites. The concentration of Brønsted acidic sites or nonframework Al on

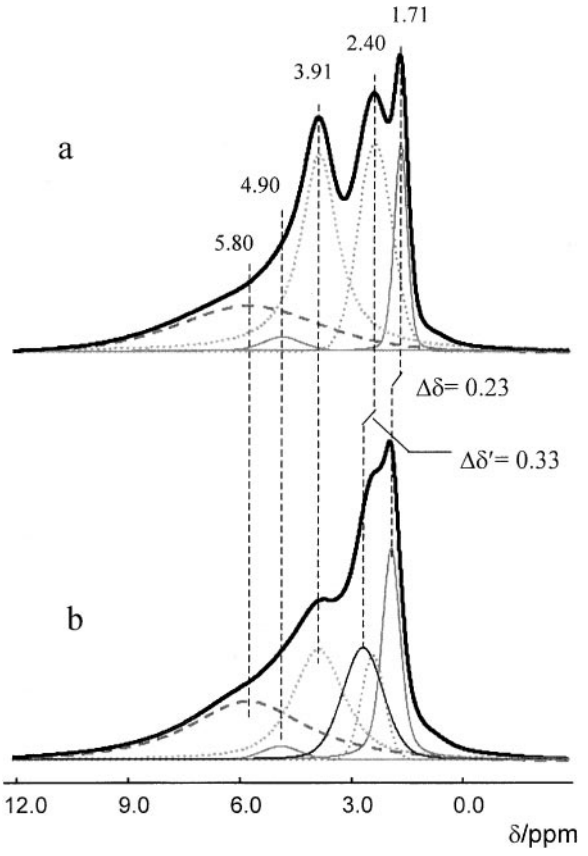

FIG. 8. ^{1}H MAS NMR and their deconvoluted spectra of the nanosized HZSM-5 zeolite before (a) and after (b) adsorption of perfluorotributyl amine, recorded with a sample spinning rate of 8 kHz and 200 scans.

the external surface of the zeolite can be calculated by

$$C_{\text{ext.surf}} = (1 - A_1/A_2) \times 100\%, \qquad [1]$$

where A_1 and A_2 denote the integral area of the peak at 3.9 or 2.4 ppm after and before adsorption of perfluorotributyl amine, respectively. Based on Eq. [1], the concentrations of Brønsted acidic sites and nonframework Al on the external surface of the Mo-loaded nanosized and microsized HZSM-5 zeolites are listed in Table 1. It is clearly shown in Table 1 that, with increasing Mo loading, the concentrations of Brønsted acidic sites and nonframework Al on the external surface of the nanosized HZSM-5 decrease from 31.7 to 4.7% and from 65.6 to 28.2%, respectively. This suggests that the decreases in the peak intensity at 3.9 and 2.4 ppm (Fig. 7b) are mainly due to the interaction of Mo species with the Brønsted acidic sites and nonframework AlOH on the external surface of nanosized HZSM-5 zeolite. However, for the microsized HZSM-5 zeolite (Table 1), its concentration of the Brønsted acidic sites on the external surface varies only from 3.5 to 2.5% as Mo loading is increased to 15 wt%. This demonstrates that the introduction of Mo species seems to have little effect on the external Brønsted acidic sites. However, the intensity of the peak at 3.9 ppm decreases with increasing Mo loading (Fig. 7a). Therefore, we speculate that some of the Mo species diffused into the lattice channels of the microsized HZSM-5 zeolite after calcination at 773 K and interacted with the internal Brønsted acidic sites. When microsized HZSM-5 was used as the support the migration of Mo species into the HZSM-5 channel is possible due to its smaller external surface area. Similar results were obtained by Lunsford *et al.* (9) and Howe *et al.* (10) in characterizing the Mo/HZSM-5 catalyst using XPS, ISS, and FT-IR techniques.

The above discussion clearly demonstrates that Mo species preferentially interact with the silanols and nonframework AlOH on the external surface of the zeolites. Both the ^{27}Al and the ^{1}H MAS NMR spectra show that Mo species and Brønsted acidic sites (i.e., framework Al) also interact. For the nanosized HZSM-5, impregnated Mo species remain predominantly on the external surface of the zeolite and interact with the external Brønsted acidic sites, but for the microsized HZSM-5, they may migrate into the zeolite channels and interact with the internal Brønsted acidic sites. The acidic sites in the zeolites may act as powerful traps for the migrated Mo species. If the Mo species strongly interact with the framework Al through an oxygen bridge after exchange with protons of the Brønsted sites, an extraction of aluminum from the zeolite framework could occur (39), as has also been proven by the ^{27}Al and ^{29}Si MAS NMR spectra mentioned above.

3.4. Catalytic Performance on the Mo/HZSM-5 Catalysts

Figure 9 shows methane conversions and aromatics selectivities for the methane dehydro-aromatization in the absence of oxygen at 973 K and a space velocity of 1500 h^{-1} after running for 1 h over the Mo/*nano*-HZ and Mo/*micro*-HZ catalysts. It was found that the conversion of methane increases significantly with increasing Mo loading. However, the optimum Mo loading for both the microsized and the nanosized HZSM-5 supports is about 6 wt%. Further addition of Mo results in a decrease in the activity and selectivity of the catalyst for the conversion of methane to aromatics (including benzene, toluene, and naphthalene). It is clearly indicated in Fig. 9 that both methane conversion and aromatics selectivity are higher for the Mo/*micro*-HZ catalyst than for the Mo/*nano*-HZ catalyst. The best activity for methane dehydro-aromatization was obtained on the microsized HZSM-5 zeolite loaded with 6 wt% Mo where methane conversion reaches 10.5% and the selectivity of aromatics is about 73%.

When comparing the results of ^{27}Al, ^{29}Si MAS, and CP/MAS NMR with the above catalytic performances on Mo/*micro*-HZ and Mo/*nano*-HZ, it seems that the formation of $Al_2(MoO_4)_3$ crystallines in the course of catalyst preparation causes the catalysts to be less active for methane

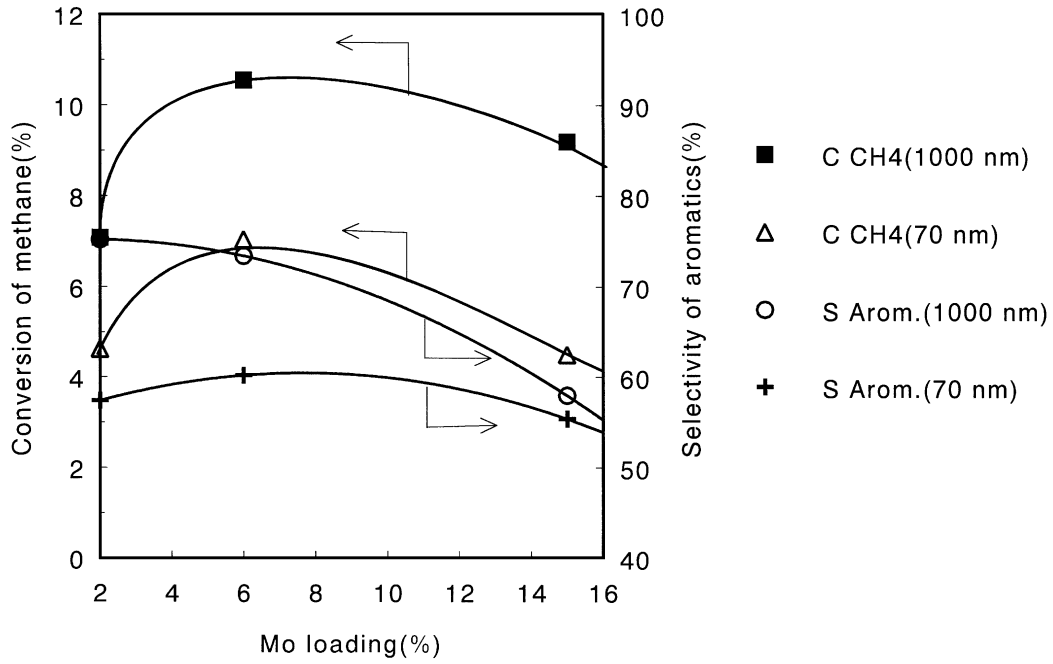

FIG. 9. Methane conversion and aromatic selectivity for CH_4 reaction over the Mo/*micro*-HZ and Mo/*nano*-HZ catalysts at 973 K and GHSV = 1500 h^{-1} after running for 1 h in the absence of oxygen.

dehydro-aromatization. Moreover, the results of ^{1}H MAS NMR before and after adsorption of perfluorotributyl amine on Mo/*micro*-HZ and Mo/*nano*-HZ demonstrate that some Mo species migrate into the channels of microsized HZSM-5 zeolite, combining with the fact that the catalytic performance of Mo/*micro*-HZ is better than that of Mo/*nano*-HZ, we suppose that the migration of some Mo species into the channels of HZSM-5 might be beneficial for the activation of methane. This may probably be due to the migrated Mo species interacted with some internal Brønsted acidic sites and weakened their acidity. A proper acidity is advantageous for the formation of benzene and toluene and for the reduction of coke. Therefore, acidity and dispersion of the Mo species as well as shape selectivity of the HZSM-5 zeolite are crucial for the conversion of methane to aromatics in the absence of oxygen (3–5, 9).

4. CONCLUSIONS

1. ^{27}Al and ^{29}Si MAS, CP/MAS NMR investigations of microsized and nanosized HZSM-5 zeolites loaded with Mo show that the Mo species and framework aluminum interact strongly. The introduction of the Mo species leads to the extraction of aluminum from the zeolite framework. With increasing Mo loading, this interaction becomes stronger on the nanosized HZSM-5 support than on the microsized HZSM-5 support and results in the formation of more nonframework aluminum resonanced at *ca.* 30 ppm in the ^{27}Al MAS NMR spectrum and finally leads to the appearance of the new $Al_2(MoO_4)_3$ crystalline phase. These new crystallines are more stable on the microsized HZSM-5 than on the nanosized HZSM-5. It seems that the formation of the $Al_2(MoO_4)_3$ crystallines causes the catalysts to become less active for methane dehydro-aromatization.

2. As proven by the selective adsorption of perfluorotributyl amine for the ^{1}H MAS NMR experiments, Mo species preferentially react with the silanols and nonframework AlOH on the external surface of the zeolites during impregnation and calcination processes.

3. For the nanosized HZSM-5 zeolite, impregnated Mo species remain predominantly on the external surface and interact with the external Brønsted acidic sites, while for the microsized HZSM-5 zeolite, they may migrate into the lattice channels and interact with the internal Brønsted acidic sites.

4. The migration of some Mo species into the zeolite channels might be advantageous for the activation of methane and the formation of aromatics such as benzene and toluene under nonoxidative conditions.

ACKNOWLEDGMENTS

The authors gratefully acknowledge the support of the National Natural Science Foundation of China and the Ministry of Science and Technology of China (the Pandeng Project).

REFERENCES

1. Wang, L., Tao, L., Xie, M., Xu, G., Huang, J., and Xu, Y., *Catal. Lett.* **21**, 35 (1993).

2. Xu, Y., Shu, Y., Liu, S., Huang, J., and Guo, X., *Catal. Lett.* **35**, 233 (1995).
3. Xu, Y., Liu, S., Wang, L., Xie, M., and Guo, X., *Catal. Lett.* **30**, 135 (1995).
4. Chen, L., Lin, L., Xu, Z., Li, Z., and Zhang, T., *J. Catal.* **157**, 190 (1995).
5. Wong, S. T., Xu, Y., and Guo, X., *Appl. Catal. A* **136**, 7 (1996).
6. Liu, S., Dong, Q., Ohnishi, R., and Ichikawa, M., *J. Chem. Soc. Chem. Commun.* 1455 (1997).
7. Solymosi, F., Cserényi, J., Szoke, A., Bansagi, T., and Oszkó, A., *J. Catal.* **165**, 150 (1997).
8. Liu, W., Xu, Y., Wong, S., Wang, L., Qin, J., and Yang, N., *J. Mol. Catal. A* **120**, 257 (1997).
9. Wang, D., Lunsford, L. H., and Rosynek, M. P., *J. Catal.* **169**, 347 (1997).
10. Zhang, J. Z., Long, M. A., and Howe, R. F., *Catal. Today* **44**, 293 (1998).
11. Weckhuysen, B. M., Wang, D., Rosynek, M. P., and Lunsford, J. H., *J. Catal.* **175**, 338 (1998).
12. Weckhuysen, B. M., Wang, D., Rosynek, M. P., and Lunsford, J. H., *J. Catal.* **175**, 347 (1998).
13. Ohnishi, R., Liu, S., Dong, Q., Wang, L., and Ichikawa, M., *J. Catal.* **182**, 92 (1999).
14. Engelhardt, G., and Michel, D., "High-Resolution Solid-State NMR of Silicates and Zeolites." Wiley, New York, 1987.
15. Bell, A. T., and Pines, A., "NMR Techniques in Catalysis," Dekker, New York, 1994.
16. Hunger, M., *Catal. Rev.-Sci. Eng.* **39**, 345 (1997).
17. Haw, J. F., and Xu, T., *Adv. Catal.* **42**, 115 (1998).
18. Zhang, W., Bao, X., Guo, X., and Wang, X., *Catal. Lett.* **60**, 89 (1999).
19. Rocha, J., and Klinowski, J., *J. Chem. Soc. Chem. Commun.* 1121 (1991).
20. Rocha, J., Carr, S. W., and Klinowski, J., *Chem. Phys. Lett.* **187**, 401 (1991).
21. Munson, E. J., Murray, D. K., and Haw, J. F., *J. Catal.* **141**, 733 (1993).
22. Man, P. P., Klinowski, J., Trokiner, A., Zanni, H., and Papon, P., *Chem. Phys. Lett.* **151**, 143 (1988).
23. Morris, H. D., and Ellis, P. D., *J. Am. Chem. Soc.* **111**, 6045 (1989).
24. Alemany, L. B., and Kirker, G. W., *J. Am. Chem. Soc.* **108**, 6158 (1986).
25. Samoson, A., Lippmaa, E., Engehardt, G., Lohse, U., and Jerschkewitz, H. G., *Chem. Phys. Lett.* **134**, 589 (1987).
26. Klinowski, J., Fyfe, C. A., and Gobbi, G. C., *J. Chem. Soc. Faraday Trans.* **81**, 3003 (1985).
27. Grobet, P. J., Geerts, H., Tielen, M., Marttens, J. A., and Jacobs, P. A., *in* "Zeolites as Catalysts, Sorbents and Detergent Builders" (H. G. Karge and J. Weitkamp, Eds.), Vol. 46, p. 721. Elsevier, Amsterdam, 1989.
28. Muller, D., Gessner, W., Behrens, H. J., and Scheler, G., *Chem. Phys. Lett.* **79**, 59 (1981).
29. Brunner, E., Ernst, H., Freude, D., Frohlich, T., Hunger, M., and Pfeifer, H., *J. Catal.* **127**, 34 (1991).
30. Loewenstein, W., *Am. Mineral.* **39**, 92 (1954).
31. Fyfe, C. A., Gobbi, G. C., Kennedy, G. J., Graham, J. D., Ozubko, R. S., Murphy, W. J., Bothner-By, A., Dadok, J., and Che, A. S., *Zeolites* **5**, 179 (1985).
32. Brunner, E., *J. Mol. Struct.* **355**, 61 (1995).
33. Beck, L. W., White, J. L., and Haw, J. F., *J. Am. Chem. Soc.* **116**, 9657 (1994).
34. Hunger, M., Freude, D., and Pfeifer, H., *J. Chem. Soc. Faraday Trans.* **87**, 657 (1991).
35. Massoth, F. E., *Adv. Catal.* **27**, 265 (1978).
36. Millman, W. S., Crespin, M., Cirillo, A. C., Abdo, J. S., and Hall, W. K., *J. Catal.* **60**, 404 (1979).
37. Take, J., Yoshioka, H., and Misono, M., *in* "Proceedings, 9th International Congress on Catalysis, Calgary 1988" (M. J. Philips and M. Ternan, Eds.), The Chem. Institute of Canada, Ottawa, 1988.
38. Zhang, W., Ma, D., Liu, X., Liu, X., and Bao, X., *J. Chem. Soc. Chem. Commun.* 1091 (1999).
39. Ezzamarty, A., Catherine, E., Cornet, D., and Hemidy, J. F., *in* "Zeolites: Facts, Figures Future" (P. A. Jacobs and R. A. van Santen, Eds.), Vol. 49, p. 1025. Elsevier, Amsterdam, 1989.